

# A Biomechanical Model of Sagittal Tongue Bending

**Vitaly J. Napadow**

Department of Health Sciences and Technology,  
Massachusetts Institute of Technology,  
77 Massachusetts Ave.,  
Cambridge, MA 02139

**Roger D. Kamm**

Department of Mechanical Engineering,  
Massachusetts Institute of Technology,  
77 Massachusetts Ave.,  
Cambridge, MA 02139

**Richard J. Gilbert<sup>1</sup>**

Department of Mechanical Engineering,  
Massachusetts Institute of Technology,  
77 Massachusetts Ave.,  
Cambridge, MA 02139

*The human tongue is a structurally complex and extremely flexible organ. In order to better understand the mechanical basis for lingual deformations, we modeled a primitive movement of the tongue, sagittal tongue bending. We hypothesized that sagittal bending is a synergistic deformation derived from co-contraction of the longitudinalis and transversus muscles. Our model of tongue bending was based on classical bimetal strip theory, in which curvature is produced when one muscle layer contracts more so than another. Contraction was modulated via mismatched thermal expansion coefficients and temperature change (to simulate muscular contraction). Our results demonstrated that synergistic contraction produced curvature and strain results which were in better correspondence to empirical results derived from tagging MRI than were the results of contraction of the longitudinalis muscle alone. This fundamental reliance of tongue bending on the synergistic contraction of its intrinsic fibers supports the muscular hydrostat theory of tongue function. [DOI: 10.1115/1.1503794]*

*Keywords:* Muscle Analog Model, Lingual Deformation

## Introduction

The human tongue is a versatile, lithe muscular organ, which is critical to such physiological tasks as mastication, swallowing and speech. In this paper, we model a primitive movement of the tongue, sagittal tongue bending. This deformation can be considered a foundation of lingual deformations seen in oral phase swallowing, wherein the tongue undergoes sagittal bending to place the tip posterior to the top row of teeth, forming an accommodation pouch in which a bolus of food is held.

The musculature of the anterior tongue (Fig. 1) is composed of intrinsic muscles, myofiber populations wholly contained in the body of the tongue and unconnected to any external bony attachments [1]. In contrast, extrinsic muscles have a bony attachment outside the tongue proper. One of the intrinsic muscles, the superior longitudinalis muscle, runs parallel to the dorsal surface of the tongue, below the thick epithelium. Below this myofiber population, lies the intrinsic core of the tongue which contains sequential sheets (in the coronal plane) of superior-inferiorly and medial-laterally directed fibers; the verticalis and transversus muscles, respectively. Below this layer is the inferior longitudinalis muscle followed by connective tissue, the lingual gland, epithelium, and a thin strip of tissue called the frenulum, which connects the anterior tongue to the floor of the mouth. The transversus, verticalis, and longitudinalis muscles also extend to the posterior tongue. The posterior tongue contains a central region of fibers originating at the mental spine of the mandible and projecting in a fan-like manner in the superior, lateral, and posterior directions (corresponding to the extrinsic genioglossus muscle). There are two major laterally inserted fiber populations, the first directed posterior and inferior (the extrinsic hyoglossus muscle) and the second directed posterior and superior (the extrinsic styloglossus muscle).

Sagittal bending is one of several primitive deformations assumed by the tongue during swallowing. Classically, superior-directed tongue bending is considered to result from contraction of the superior longitudinalis muscle alone [2]. In contrast, we hypothesized that sagittal bending may be better depicted by the

combined contractions of the transversus and the longitudinalis muscles. This theory converges well with the depiction of the tongue as a muscular hydrostat [2], an organ that functions by deforming in a plane orthogonal to the contraction axis by conservation of volume. One of the goals of this modeling effort was to evaluate the extent to which combined contractions of the transversus and longitudinalis muscle account for sagittal tongue bending. In order to validate our model, we compared the theoretical results to previously published empirical measurements obtained by Tagging MRI [3].

The theoretical model of tongue bending was based on classical bimetal strip theory [4,5], which is typically applied in electrical thermostat switch design. Bimetal strip theory applies to the case in which two metals of different thermal expansion coefficient are bonded together at an interface and are subjected to a temperature change [6]. Under these conditions, the thermal expansion response of each layer differs, yet the bond between the layers remains fixed. Thus, the only way for the strip to accommodate the differing expansions is to bend. In the case of sagittal tongue bending, a beam curvature is produced when one muscle layer (specifically the longitudinalis muscle) contracts more so than the other layers. Hence, if muscular contractile strain can be considered analogous to thermal contractile strain, the layered muscular sandwich within the tongue can be adequately modeled by a classical bimetal strip. One strip layer was composed of the superior longitudinalis muscle and was bonded to the other layer, composed of the transversus and verticalis muscles. Once the strip was subjected to a temperature change, contraction of the longitudinalis and transversus muscles was accomplished by specifying the directionally dependent thermal expansion coefficients for the different layers.

Previous models of lingual muscular activity have emphasized relatively simple geometry and few elements, incorporating realistic activation and dynamics properties [7], as well as multi-element finite element models, incorporating correct three-dimensional geometry and viscoelastic constitutive properties [8]. The geometry of the former model was particular to certain reptilian tongues and significantly divergent from human tongues. The latter model's complexity provided greater flexibility of deformation, yet introduced model instability when setting optimization functions. Still other models have attempted to model two-dimensionally the intrinsic and extrinsic behavior of the human

<sup>1</sup>Corresponding author: Richard J. Gilbert, Department of Mechanical Engineering, Massachusetts Institute of Technology, 77 Massachusetts Avenue, 41-211, Cambridge, MA 02139, Phone: 617-254-6875, Fax: 617-253-2249, E-mail: rgilbert@mit.edu

Contributed by the Bioengineering Division for publication in the JOURNAL OF BIOMECHANICAL ENGINEERING. Manuscript received March 2001; revised manuscript received June 2002. Associate Editor: M. S. Sacks.

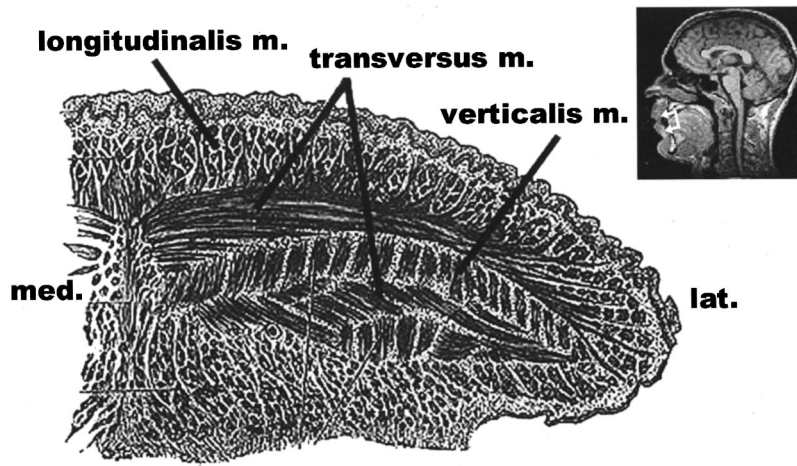


**Fig. 1** The intrinsic musculature of the human tongue, as depicted by histological axial cross-section. The medial and lateral locations are shown. The longitudinalis m. runs along the tongue's long axis; while the transversus m. (extending medial-laterally) and verticalis m. (extending inferior-superiorly) are seen in-plane in this figure. Approximate location through anterior tongue is visualized in the inset MRI sagittal image (upper right). [Image adapted from Gray's Anatomy by Henry Gray, Crown Publishers, Inc., 1976.]

tongue by subdividing the muscular organ into gross directional myofiber elements [9,10]. While not wholly parcellating the organ as a finite element model, these models attempted to retain some of the flexibility of a generalized description, while still somewhat limiting the scope of investigation. For instance, both of these models utilized linear elastic isotropic constitutive descriptions. Model comparisons to empirical results were lacking. However, the Hashimoto and Suga model, which involved tongue deformations in the production of vowel sounds, was validated by comparison to cine x-ray images.

Our model differed from past investigations in that it was an analog model comparing the tongue to a common mechanical engineering device, a bi-layered beam with differing thermal expansion properties. Secondly, we validated our model with not just gross geometry (i.e., global curvature through cine x-ray), but with internal deformation metrics (i.e. strain measurements through the cross-section with Tagging MRI). This model was created to answer a specific question: what muscular elements of the human tongue are involved in the common tongue deformation, sagittal bending toward the hard palate.

## Methods

**Development and Validation of Analog Model.** A mechanical analog model was developed and compared to strain measurement data derived from a prior tagging MRI study [3]. In this study, we explored two different mechanisms by which the tongue might achieve sagittal bending in vivo. One mechanism required the superior longitudinalis muscle to contract without concurrent contraction of the inferior longitudinalis muscle (otherwise the tongue would simply shorten), thereby producing a longitudinal strain gradient through the cross-section as well as a curved global deformation, consistent with sagittal bending. By an alternative mechanism, superior longitudinalis muscle contraction was aided by contraction of the transversus muscle, which produced an anticlastic curvature about the medial-lateral axis, thereby augmenting sagittal bending. The existence of independent contractions of the muscular components of the intrinsic mammalian tongue was acknowledged in a study of motor unit innervation [11]. The authors concluded that the orthogonally oriented muscle sheets of the core intrinsic muscles (transversus and verticalis muscles) appeared to be individually innervated by separate branches of the trigeminal (sensory) and hypoglossal (motor) nerves.

In order to address this mechanistic distinction, we modeled the tongue as a composite beam, which has an initial curvature in its rest configuration, and then undergoes a change in curvature due to dissimilar contraction patterns of the beam elements. The top beam element (beam 1) represents the longitudinalis muscle layer, while the bottom beam element (beam 2) represents the intrinsic core of the tongue which is composed of the transversus and verticalis muscles. Muscular contraction has been simulated in the bimetal strip model by assigning different thermal expansion coefficients ( $\alpha(\mathbf{x})$ ) to the different beam layers. Using this approach, we assessed the relative contribution of the transversus and longitudinalis muscles on sagittal bending.

The bimetal strip bent beam analog solution is derived from the classical mechanics theory [6,12] with several modifications. The following assumptions were made in order to produce a set of governing equations which could be readily solved by analytical methods: (1) cross-sections originally planar and perpendicular to the beam's curved long axis, remain planar and perpendicular to the new curved long axis after deformation, (2) contraction does not produce shear deformation, i.e. only pure bending is modeled (Bernoulli-Euler beams), (3) the two beams are connected by rigid plates at the ends, hence concentrated force at the ends is transformed into a linear stress variation through the cross-section (otherwise shear deformation occurs at the ends, conflicting with assumption 1), (4) the solutions for concurrent contractions of the longitudinalis and transversus muscles can be superimposed, and lastly (5) both beams were assumed to be comprised of isotropic, linear elastic materials with orthotropic thermal expansion coefficients.

In classical bimetal strip theory, a composite beam is formed by two beams of different material composition bonded at an interface. The two beams can have different thickness ( $h_1, h_2$ ), Young's modulus ( $E_1, E_2$ ), Poisson's ratio ( $\nu_1, \nu_2$ ), and thermal expansion coefficient ( $\alpha_1, \alpha_2$ ). Table 1 contains definitions of the relevant parameters used in the model. If  $\alpha_1 > \alpha_2$  and there is a temperature drop  $\Delta T$ , beam 1, if unencumbered, would contract to a greater degree than beam 2. However, since the two beams are bonded together, beam 2 restricts beam 1's contraction by applying shearing forces at the bonding interface. If each beam is then taken as a separate free-body diagram, the shearing forces, since they are not applied centrally, produce bending moments on each beam. These two moments may be different since the beams can

**Table 1 Model parameter definitions**

Parameter	Definition
$h_1$ :	Height of beam 1 (superior longitudinalis m.)
$h_2$ :	Height of beam 2 (transversus and verticalis m.)
$h$ :	Total height of bimetal strip ( $h=h_1+h_2$ )
$b$ :	Width of beam
$L$ :	Length of beam (measured along convex edge)
$E_1$ :	Young's Modulus of beam 1
$E_2$ :	Young's Modulus of beam 2
$\nu_1$ :	Poisson's ratio for beam 1
$\nu_2$ :	Poisson's ratio for beam 2
$\alpha_1$ :	Thermal expansion coefficient for beam 1
$\alpha_2$ :	Thermal expansion coefficient for beam 2
$\Delta T$ :	Temperature change experienced by the bimetal strip
$R_o$ :	Initial radius of curvature to bimetal strip neutral axis
$k_o$ :	Initial curvature ( $k_o=1/R_o$ )
$R_{o1}$ :	Initial radius of curvature to beam 1 neutral axis
$R_{o2}$ :	Initial radius of curvature to beam 2 neutral axis
$R_b$ :	Radius of curvature induced by the bending moment
$R_f$ :	Final radius of curvature of bimetal strip neutral axis
$P_1$ :	Axial load applied to beam 1
$P_2$ :	Axial load applied to beam 2
$M_1$ :	Moment applied to beam 1
$M_2$ :	Moment applied to beam 2

have different thickness; however, equilibrium dictates that the sum of the moments must equal the moment-couple created by the shearing forces acting centrally on each beam (Fig. 2):

$$P_1 = P_2 = P \tag{1}$$

$$M_1 + M_2 = P_1 \left( \frac{h_1}{2} \right) + P_2 \left( \frac{h_2}{2} \right) = P \left( \frac{h}{2} \right) \tag{2}$$

Constitutive relations describe the relationship of material deformation to loading. For the case of a curved beam bimetal strip problem, the relationship between moment and curvature can be

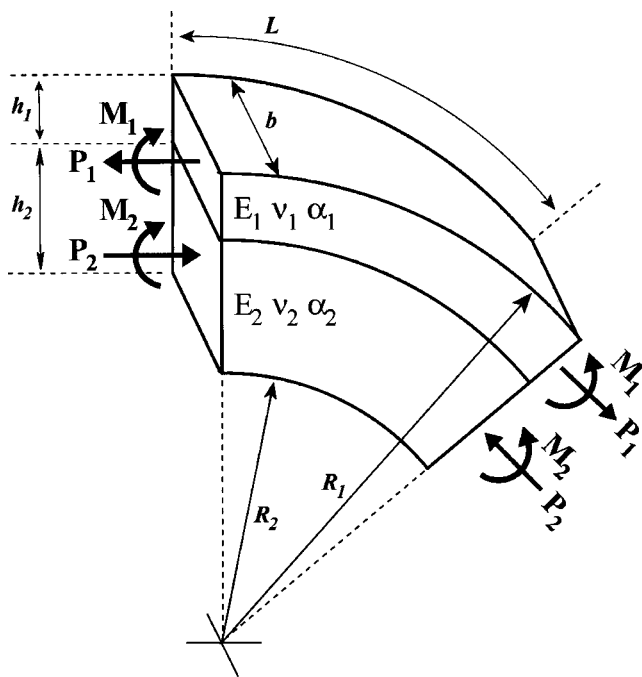


**Fig. 2 Analog model defined by two materials bonded together at an interface. The bimetal strip is initially concave-downward; each material is constitutively defined by its material properties and spatial dimensions (see Table 1). Upon contraction of the top material, the “bimetal strip” is subjected to the forces and moments defined on the schematic.**

found by integrating the differential moment produced by the bending stress distribution across the indicated cross-section.

$$M = \int y \sigma dA \tag{3}$$

Since the curvature changes that are anticipated in the tongue model are very large, linear strain definitions could not be used. Instead, we chose to use Green's strain,  $\epsilon = 1/2(U^2 - 1)$ , to define non-linear bending strain in a curved beam (see Appendix 1 for derivation):

$$\epsilon = \frac{1}{2} \left[ \left( 1 + \frac{yR_o}{y+R_o} \left( \frac{1}{R_b} \right) \right)^2 - 1 \right] \tag{4}$$

where y is the distance from the neutral axis,  $R_o$  is the original radius of curvature to the neutral axis of the curved beam (see Appendix 2 for derivation of  $R_o$ ), and  $R_b$  is the radius of curvature caused by the bending moment, M. Using equation (4) and assuming that tongue musculature behaves as a linear elastic material, equation (3) can be evaluated analytically:

$$M = \frac{Eb}{2(1-\nu^2)} \left[ (R_1 + R_2)hR_o - 4hR_o^2 + 2R_o^3 \ln \frac{R_2}{R_1} \right] \left( \frac{1}{R_b} \right) + \frac{Eb}{4(1-\nu^2)} \left[ (R_1 + R_2)hR_o^2 - 6hR_o^3 + 6R_o^4 \ln \frac{R_2}{R_1} \right] + 2R_o^5 \left( \frac{1}{R_2} - \frac{1}{R_1} \right) \left( \frac{1}{R_b^2} \right) \tag{5}$$

where b is the width of the beam, and  $R_1$  and  $R_2$  are the inner and outer radii, respectively, of a beam initially bent concave down. Note that M is defined to be positive clockwise. Hence, the non-linear strain definition produces a moment-curvature relation that is itself quadratic.

In order to solve for the curvature produced by a given contraction, a compatibility relation must be imposed at the interface of the two beams. That is, for the two beams to remain bonded at the interface, the longitudinal strain experienced by the lower plane of the upper beam and that experienced by the upper plane of the lower beam must be equal. The longitudinal strain is the sum of the thermal, axial,<sup>1</sup> and bending strain. At the interface,  $y_1 = R_2 + h_2 - R_{o1}$  and  $y_2 = R_2 + h_2 - R_{o2}$ ; which can be substituted into equation (4) to derive the bending strain. Thus, strain matching can be expressed mathematically as:

$$\epsilon_{xx_1}(R_2 + h_2) = \epsilon_{xx_2}(R_2 + h_2) \alpha_1 \Delta T + \frac{P}{E_1 h_1 b} + \frac{1}{2} \left[ \left( 1 + \frac{(R_2 + h_2 - R_{o1})R_{o1}}{R_2 + h_2} \left( \frac{1}{R_b} \right) \right)^2 - 1 \right] = \alpha_2 \Delta T - \frac{P}{E_2 h_2 b} + \frac{1}{2} \left[ \left( 1 + \frac{(R_2 + h_2 - R_{o2})R_{o2}}{R_2 + h_2} \left( \frac{1}{R_b} \right) \right)^2 - 1 \right] \tag{6}$$

where  $R_{o1}$  and  $R_{o2}$  are the radius of curvature to the neutral axis of beam 1 and beam 2, respectively. Finally, the change in curvature produced in the bimetal strip can be found by combining equation (6) with equation (2) (in elasticity theory, this is a combination of equilibrium, constitutive relations, and compatibility). The radius of curvature produced by the bending moments acting on the strip can be found by solving the quadratic equation:

<sup>1</sup>The axial strain is defined by  $\epsilon = \sigma/E = P/Ehb$

$$\left[ \frac{(R_2+h_2-R_{o_1})^2 R_{o_1}^2 - (R_2+h_2-R_{o_2})^2 R_{o_2}^2}{(R_2+h_2)^2} - \frac{4(B_1+B_2)}{h} \left( \frac{1}{E_1 h_1} + \frac{1}{E_2 h_2} \right) \right] \frac{1}{R_b^2} + \left[ \frac{2[(R_2+h_2)(R_{o_1}+R_{o_2})+R_{o_2}^2-R_{o_1}^2]}{R_2+h_2} - \frac{4(A_1+A_2)}{h} \left( \frac{1}{E_1 h_1} + \frac{1}{E_2 h_2} \right) \right] \frac{1}{R_b} + 2(\alpha_1 - \alpha_2)\Delta T = 0 \quad (7)$$

where

$$A_1 = \frac{E_1}{2(1-\nu_1^2)} \left[ (R_1^2 - (R_2+h_2)^2)R_{o_1} - 4h_1 R_{o_1}^2 + 2R_{o_1}^3 \ln \left( \frac{R_1}{R_2+h_2} \right) \right]$$

$$A_2 = \frac{E_2}{2(1-\nu_2^2)} \left[ ((R_2+h_2)^2 - R_2^2)R_{o_2} - 4h_2 + 2R_{o_2}^2 + 2R_{o_2}^3 \ln \left( \frac{R_2+h_2}{R_2} \right) \right]$$

$$B_1 = \frac{E_1}{4(1-\nu_1^2)} \left[ (R_1^2 - (R_2+h_2)^2)R_{o_1}^2 - 6h_1 R_{o_1}^3 + 6R_{o_1}^4 \ln \left( \frac{R_1}{R_2+h_2} \right) + 2R_{o_1}^5 \left( \frac{1}{R_1} - \frac{1}{R_2+h_2} \right) \right]$$

$$B_2 = \frac{E_2}{4(1-\nu_2^2)} \left[ ((R_2+h_2)^2 - R_2^2)R_{o_2}^2 - 6h_2 R_{o_2}^3 + 6R_{o_2}^4 \ln \left( \frac{R_2+h_2}{R_2} \right) + 2R_{o_2}^5 \left( \frac{1}{R_2+h_2} - \frac{1}{R_2} \right) \right] \quad (8)$$

$A_1$  and  $A_2$  are derived from the constant in front of the linear term in equation (5) for beam 1 and beam 2, respectively.  $B_1$  and  $B_2$  are derived from the constant in front of the quadratic term in equation (5) for beam 1 and beam 2, respectively. A sensitivity analysis of these equations was completed wherein the effect of varying a given parameter was evaluated by the variability induced on the computed curvature.

The final radius,  $R_f$ , of the bimetal strip can now be found. A beam with initial curvature  $R_o$ , undergoing bending described by a change in curvature of radius  $R_b$ , assumes a final radius defined by:

$$\frac{1}{R_f} = \frac{1}{R_b} + \frac{1}{R_o} \quad (9)$$

Model parameters were derived principally from MRI images and the Visible Human: Male database [13] (Fig. 4, Table 2). MRI images of the same human subject from whom the empirical strain data were derived, were used to measure total height of beam,  $h$ ; width of beam,  $b$ ; length of beam,  $L$ ; initial curvature,  $R_o$ ; and final curvature,  $R_f$  (which was used to help corroborate model output). The initial and final curvatures were measured by fitting a circle to a set of points digitized along a contour (Fig. 5). This was accomplished by minimizing the rms error while varying the circle radius and center location. A mid-sagittal slice from the Visible Human Male database was used to find the percentage composition of dorsal epithelium, superior longitudinalis muscle, transversus/verticalis muscles, inferior longitudinalis muscle, lingual gland and frenulum in a transverse x-section through the anterior tongue (approximate location from which the empirical strain data was derived). These data were used to find the heights

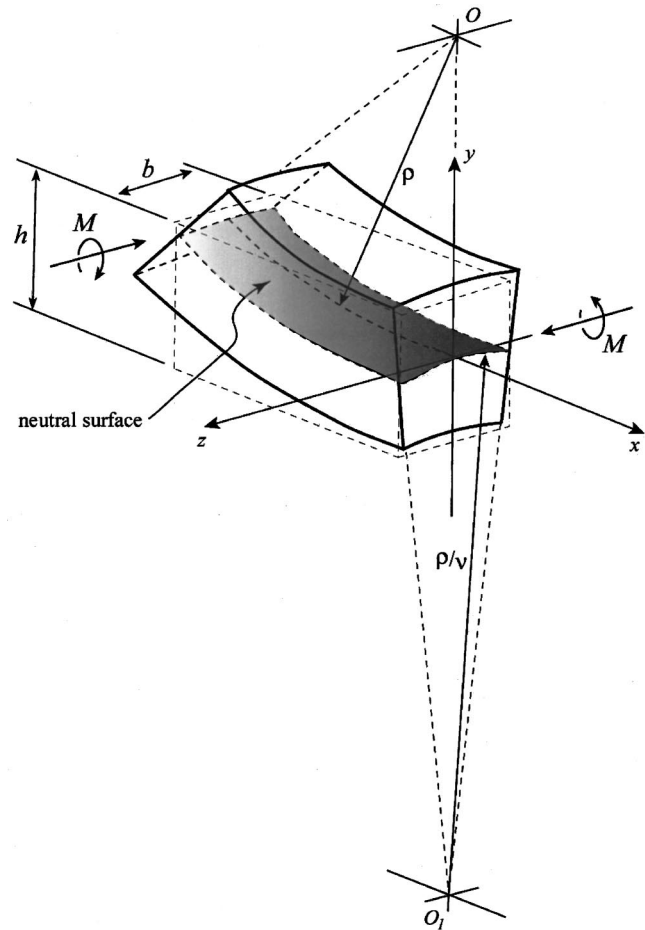


**Fig. 3** The phenomenon of anticlastic curvature arises from Poisson effects. When a beam is bent, the concave edge is under longitudinal compression, while the convex edge is under longitudinal tension. Poisson's effect dictates that the contracted edge must expand orthogonally, while the edge under tension must contract orthogonally. This requirement creates a curvature (the anticlastic curvature) which is itself in a plane orthogonal to the plane of primary bending.

of the individual beams,  $h_1$  and  $h_2$ . The Young's Modulus,  $E$ , of contracted ( $E=0.01$  MPa) and relaxed muscle ( $E=0.006$  MPa) was found from other tongue models in the literature [10] and material test results [14]. Finally, muscle contraction was modeled by assigning specific values to the thermal expansion coefficients of each beam. Due to the lack of adequate data on human tongue muscle, results from the frog (*Rana pipiens*) sartorius muscle were used [15]. The strain of muscular contraction was found to be  $-0.3$  using the length changes ( $I_{new}/I_o=0.7$ ) reported by this reference for isotonic contractions under low load. Thus, if the temperature change,  $\Delta T$ , is set to  $-1^\circ\text{C}$ , contracted muscle was defined by a thermal expansion coefficient,  $\alpha$ , equal to  $0.3^\circ\text{C}^{-1}$ , while uncontracted muscle was defined by an  $\alpha$  equal to  $0^\circ\text{C}^{-1}$ .

Contraction of the superior longitudinalis muscle produces bending in the x-y plane. However, due to the existence of Poisson's effects, an anticlastic curvature in the beam is formed in the y-z plane (Fig. 3). This curvature (which can be seen when bending a common rectangular rubber eraser) is equal to  $-\nu/\rho$ , where  $\rho$  is the radius of curvature for bending in the x-y plane and  $\nu$  is Poisson's ratio, which was set to  $1/2$ , corresponding to an incompressible material. Tissue incompressibility is commonly assumed in tongue models [7,8] as the tissue is highly aqueous, giving the

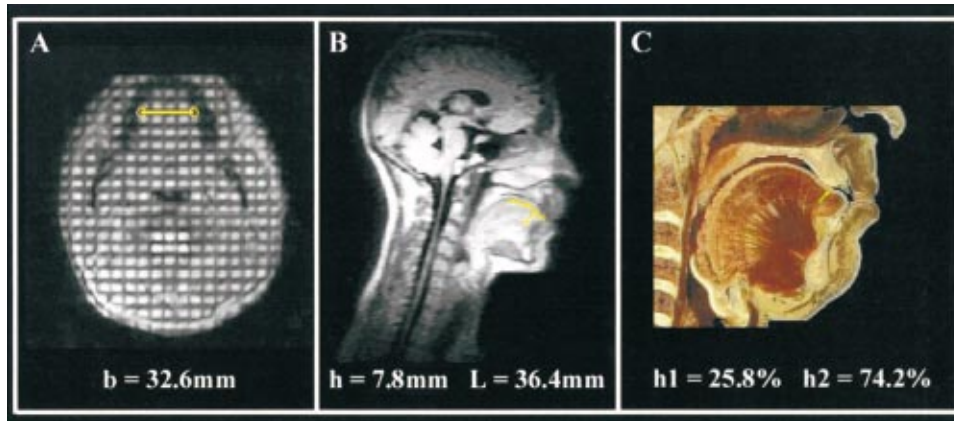


**Fig. 4** The spatial parameters used in the model were derived from either MRI images of the tongue, or from the Visible Human: Male database. (A) Coronal view MRI image (with tag lines superimposed) of the tongue depicting the width,  $b$ , of the tissue in the mid-anterior position, 32.6 mm. (B) Sagittal view MRI image of the tongue depicting the functional length (along its curvature) of the anterior tongue, 36.4 mm, and the composite height,  $h$ , 7.8 mm. (C) Sagittal view, cross-section of the muscular structure of the anterior tongue, derived from the Visible Human database, showing the relative composition percentage of the longitudinalis (25.8%) and transversus (74.2%) muscle layers.

**Table 2** Model parameter values

Parameter	Value	Source
$h_1$ :	$2.0 \pm 0.4$ mm	Visible Human data, MRI
$h_2$ :	$5.8 \pm 0.4$ mm	Visible Human data, MRI
$b$ :	$30.0 \pm 0.6$ mm	MRI
$L$ :	$35.0 \pm 0.6$ mm	MRI
$E_1$ (run 1):	0.01 MPa	Duck, 1990
$E_2$ (run 1):	0.006 MPa	Duck, 1990
$E_1$ (run 2):	0.01 MPa	Duck, 1990
$E_2$ (run 2):	0.01 MPa	Duck, 1990
$\nu_1$ :	0.5	Duck, 1990
$\nu_2$ :	0.5	Duck, 1990
$\alpha_{1-x}$ (run 1):	$0.3^\circ\text{C}^{-1}$	Matsumoto, 1967
$\alpha_{2-x}$ (run 1):	$0^\circ\text{C}^{-1}$	Matsumoto, 1967
$\alpha_{1-z}$ (run 1):	$0^\circ\text{C}^{-1}$	Matsumoto, 1967
$\alpha_{2-z}$ (run 1):	$0^\circ\text{C}^{-1}$	Matsumoto, 1967
$\alpha_{1-x}$ (run 2):	$0.3^\circ\text{C}^{-1}$	Matsumoto, 1967
$\alpha_{2-x}$ (run 2):	$0^\circ\text{C}^{-1}$	Matsumoto, 1967
$\alpha_{1-z}$ (run 2):	$0^\circ\text{C}^{-1}$	Matsumoto, 1967
$\alpha_{2-z}$ (run 2):	$0.3^\circ\text{C}^{-1}$	Matsumoto, 1967
$\Delta T$ :	$-1^\circ\text{C}$	Matsumoto, 1967
$k_0$ :	$28.5 \text{ m}^{-1}$	MRI

tongue its capability to behave as a muscular hydrostat.<sup>2</sup> Intuitively, the anticlastic curvature can be explained by the fact that the concave edge of a bent beam is in compression along the  $x$ -direction, while the convex edge is in tension along the  $x$ -direction. Thus, by Poisson's effect, the concave edge must be in tension along the  $z$ -direction while the convex edge must be in compression along the  $z$ -direction. The consequence is that a secondary curvature is formed in the beam in the  $y$ - $z$  plane; this curvature is called the anticlastic curvature. In fact, it is this curvature that explains how contraction of the transversus muscle can augment the contraction of the superior longitudinalis muscle in producing sagittal bending ( $x$ - $y$  plane) of the tongue. Contraction of the transversus muscle produces a curvature in the  $y$ - $z$  plane, and can be modeled in a similar manner by a bimetal strip analog. In addition, this contraction produces an anticlastic curvature, this time in the  $x$ - $y$  plane, which augments sagittal tongue bending. In

<sup>2</sup>Experimental techniques such as x-ray diffraction have been used to confirm skeletal muscle incompressibility [16], while studies on frog sartorius muscle have demonstrated volume decreases of less than 0.01% [17].

our model, superposition was used to combine the effects of superior longitudinalis and transversus muscle contraction.

The results of both of the tested contraction scenarios (superior longitudinalis muscle alone and both superior longitudinalis and transversus muscles) was visualized with MATLAB (The Mathworks, Inc., Massachusetts, USA) by a bent beam graphic showing the modeled beam in its final, contracted configuration. Beam deflection was tracked by visualizing the deflection of 75 points defining the convex, concave, and interfacial contours.

**Correlation of Analog Model With Empirical Data (Tagging MRI).** Corroboration of theoretical results with empirical results was accomplished by both comparing the final curvature achieved in modeled and real deflection (MRI); as well as by comparing the longitudinal strains calculated across the tongue cross-section in the model with the longitudinal strains derived from the Tagging MRI data for sagittal bending (averaged data from  $n = 5$  subjects). The MRI data were taken from the anterior tongue within the portion corresponding anatomically to the superior longitudinalis and transversus muscles. This portion was deduced by cross-sectional percentage measurements from the Visible Human: Male data.

Tagging MRI has been previously used to derive qualitative and quantitative measures of internal tissue deformation [3,18,19]. In brief, Tagging MRI is a non-invasive NMR tagging technique that allowed for the selective saturation of bands of magnetic spins in resting tongue tissue [20–22]. These bands were localized along the antero-posterior and superior-inferior directions of the mid-sagittal plane, resulting in a square rectilinear grid. As the tongue tissue deformed, the previously rectilinear grid also deformed, and axial and shear strains relative to the rest condition were determined by imaging the tongue in its deformed state, thereby tracking the relative displacement of triangular element nodes defined by MR tag line intersections.

## Results

The results of this analysis demonstrated that sagittal tongue bending could be adequately represented by an analog beam model, and could, in fact, be depicted in terms of the contractions of the tongue's constituting myofiber populations.

From its initial curved state, the tongue was found to reverse its curvature under both the "superior longitudinalis muscle only" contraction scenario, as well as the scenario wherein both the

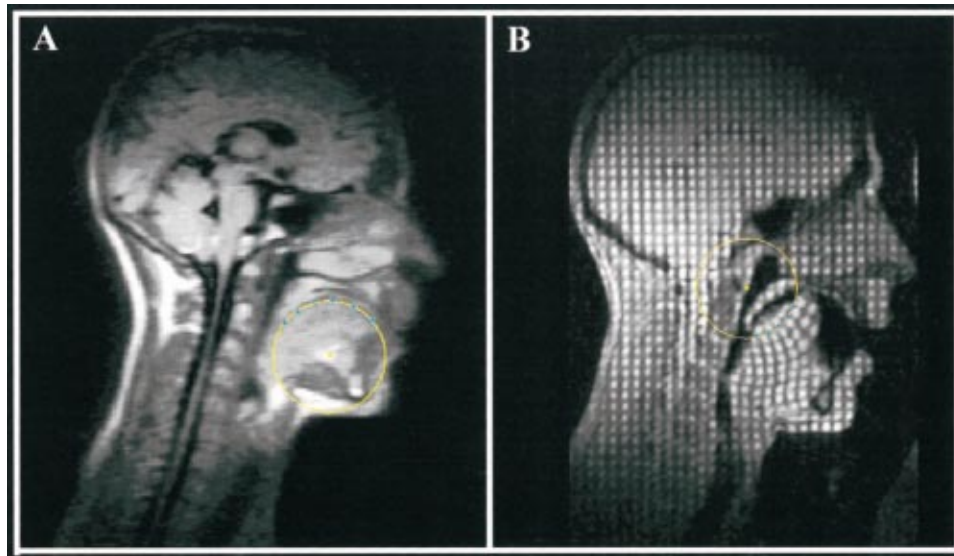


**Fig. 5** The initial (A) and final (B) tongue curvatures were measured by fitting a circle to a set of points digitized along the approximate contour of the longitudinalis/transversus interface. The best-fit circle was derived by minimizing the rms error while varying circle location and radius. MRI images used were from the same subject.

superior longitudinalis and transversus muscles contract (Table 3, Fig. 6). Positive curvature is defined as concave down, while negative curvature is defined as concave up (i.e. sagittal tongue bending). Under the condition of longitudinalis muscle contraction alone, the moment produced by the contraction induced a curvature change of  $-46.9 \text{ m}^{-1}$ , which resulted in a final curvature of  $-18.4 \text{ m}^{-1}$ . When compared to the final curvature measured from the empirical tagging MRI data ( $-30.9 \text{ m}^{-1}$ ), this scenario was found to have a percent error of 40%. However, under the condition of combined longitudinalis and transversus muscle contraction, the moment produced by the synergistic contractions induced a curvature change of  $-58.8 \text{ m}^{-1}$ , which resulted in a final curvature of  $-30.4 \text{ m}^{-1}$ . When compared to the empirical final curvature, this scenario had better correspondence (percent error of less than 2%).

Cross-sectional longitudinal strain ( $E_{xx}$ ) and medial-lateral strain ( $E_{zz}$ ) distributions calculated from the model were also compared with empirical data taken from the tagging MRI study (Fig. 7). The experiments showed that longitudinal strain was contractile ( $-0.17$ ) at a location close to the interface of the longitudinalis muscle layer and transversus/verticalis muscle layer. Near the inferior edge of the transversus/verticalis muscle layer, the longitudinal strain was 0.44. For the longitudinalis muscle only contraction scenario, theoretical longitudinal strains ( $E_{xx}$ ) ranged from  $-0.26$  at the superior edge of the longitudinalis muscle layer

(most negative) to 0.10 at the inferior edge of the transversus/verticalis muscle layer. Medial-lateral (or through-plane) strains ( $E_{zz}$ ) ranged from 0.13 at the superior edge of the longitudinalis muscle layer to  $-0.05$  at the inferior edge of the transversus/verticalis muscle layer. For the longitudinalis and transversus muscle contraction scenario, theoretical longitudinal strains ( $E_{xx}$ ) ranged from  $-0.19$  at the superior edge of the longitudinalis muscle layer to 0.27 at the inferior edge of the transversus/verticalis muscle layer. Medial-lateral (or through-plane) strains ( $E_{zz}$ ) ranged from 0.04 at the superior edge of the longitudinalis muscle layer to  $-0.41$  at the inferior edge of the transversus/verticalis muscle layer. Residual errors ( $\sqrt{(\epsilon_{\text{theory}} - \epsilon_{\text{meas}})^2}$ ) were calculated for longitudinal and medial-lateral strain profiles for both contraction scenarios. For longitudinal strain, the average error was 0.20 for the longitudinalis-only contraction and 0.13 for the transversus/longitudinalis contraction. For medial lateral strain there was not a significant difference (0.18 for the former to 0.17 for the latter) in average residual error. Again, the agreement with empirical results (both quantitative and qualitative) was closer when both muscles were activated (Fig. 6).

A sensitivity analysis of the equations involved in the model was completed wherein the effect of varying a given model parameter  $\pm 50\%$  was evaluated by the variability induced on the computed curvature (the curvature produced by the contraction) (Fig. 8). As this analysis is of the governing equations of the model (which were similar for both scenarios), the sensitivity analysis was performed on the “longitudinalis muscle only” contraction scenario. This analysis showed that curvature was most sensitive to  $\alpha_1$ , the thermal expansion coefficient of beam 1 (the beam containing the superior longitudinalis muscle), and  $h_2$ , the height of beam 2 (the beam containing the transversus and verticalis muscles). The curvature was less sensitive to  $E_1$ , the Young’s modulus of beam 1,  $E_2$ , the Young’s modulus of beam 2, and  $h_1$ , the height of beam 1. Finally, the curvature produced by superior longitudinalis muscle contraction was very minimally sensitive to  $R_o$ , the initial curvature of the strip.

## Discussion

The human tongue is a structurally heterogeneous and extremely flexible organ with a seemingly infinite number of degrees of freedom. In this modeling effort, our purpose was to gain in-

**Table 3** Simulation results

	Longitudinalis m. only Contraction	Longitudinalis and Transversus m. Contraction
Initial curvature ( $k_o = 1/R_o$ )	$28.5 \pm 1.7 \text{ m}^{-1}$	$28.5 \pm 1.7 \text{ m}^{-1}$
Curvature induced by contraction ( $k_b$ )	$-46.9 \text{ m}^{-1}$	$-58.8 \text{ m}^{-1}$
Final curvature (simulated $k_f$ )	$-18.4 \text{ m}^{-1}$	$-30.4 \text{ m}^{-1}$
Final curvature (empirical $k_f$ )	$-30.9 \pm 1.7 \text{ m}^{-1}$	$-30.9 \pm 1.7 \text{ m}^{-1}$
% Error (simulation to empirical)	40%	2%

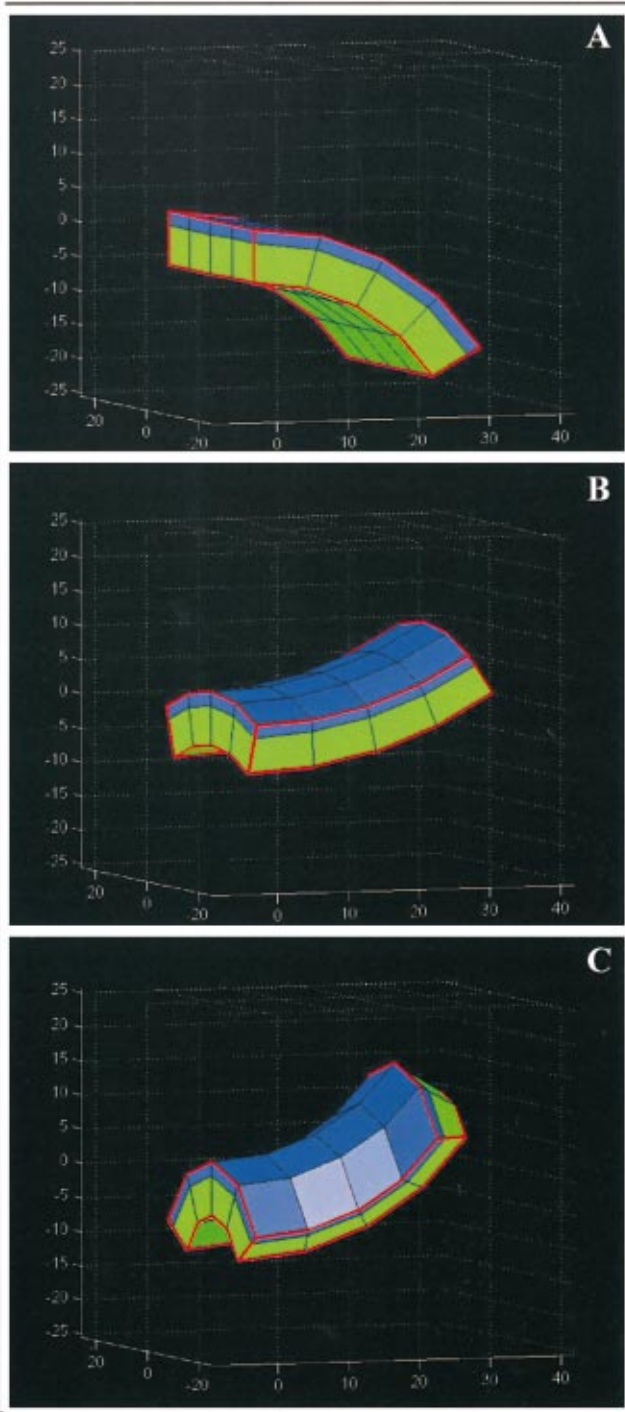


**Fig. 6** Shown are the graphic representations of the 3D model of the tongue in the (A) initial configuration, (B) final configuration for longitudinalis only contraction, and (C) final configuration for synergistic longitudinalis and transversus muscle contraction. The initially concave-down bent beam was effectively straightened by longitudinalis muscle contraction, and achieved maximal bending with synergistic longitudinalis/transversus muscle contraction.

sight into the mechanisms of a single, fundamental deformation, sagittal tongue bending. A better understanding of this basic maneuver could lead to a better understanding of some of the more complex deformations associated with human speech and swallowing.

We explored two contraction scenarios to see which best ap-

proximates actual tongue bending (as determined by tagging MRI). Both the “superior longitudinalis muscle only” contraction scenario, and the synergistic “longitudinalis and transversus muscle” contraction scenario produced a change in curvature wherein the tongue switched conformation from concave down to concave up. However, in order for the tongue tip to achieve the strain pattern and curvature associated with a fully bent configuration, approximating the hard palate (as shown by tagging MRI), co-contraction of the superior longitudinalis and transversus muscles was necessary (Table 3).

Longitudinalis muscle contraction alone was sufficient to cause tongue straightening, an action important for anterior protrusion. However, our results demonstrated that in order for the tongue to achieve the more extreme sagittal curvature associated with hard palate contact, maximal efforts from both the longitudinalis and transversus myofiber populations were necessary. Examination of the cross-sectional strain field revealed that the anterior tongue experiences large longitudinal tensile strains,  $E_{xx}$ , in the range of 44% at the inferior border of the transversus muscle layer. These strains were not well approximated by contraction of the longitudinalis muscle alone. In contrast, the strain values predicted by synergistic contraction of the muscle layers more closely approximated the experimental values for strain and curvature. It was notable, however, that even the synergistic strain values shown by the model underestimated actual longitudinal strain. We speculate that the larger longitudinal strain values seen in the empirical data may very well have been exaggerated by secondary effects, such as verticalis muscle co-contraction, which, while not augmenting global curvature, would produce greater tensile longitudinal strain. Such secondary effects were not accounted for in the current model.

Our data demonstrate that the large contractile medial-lateral (through-plane) strains,  $E_{zz}$ , measured from the tagging MRI data were not adequately modeled by the contraction of the longitudinalis muscle alone. Medial-lateral contraction occurred only through Poisson’s effects for this scenario, and produced the anti-elastic curvature. However, under the synergistic contraction scenario, medial-lateral contraction (especially in the transversus/verticalis muscle layer) occurred primarily due to active contraction of the transversus musculature. The model produced contractile strains which overestimated slightly the actual contractile deformation. This may have resulted from the model assumption that the entire transversus muscle layer contracts uniformly. In reality, contraction is most likely modulated such that the superior portion of this layer contracts less than the inferior portion. This would maximize the curvature producing effects of muscle contraction. Since the height of this layer is significantly greater than the longitudinalis muscle layer (5.8 mm compared to 2.0 mm), not accounting for gradations in transversus muscle contraction could have produced this overestimate in medial-lateral contraction strain, as well as the underestimation in tensile strain in the longitudinalis muscle layer.

In order to gain a better understanding of which parameters have greatest influence on tissue deformation, the analog model was dissected along its governing equations. This was important as the various parameters employed by the model had different degrees of measurement error. Our sensitivity study was accomplished by varying several key parameters by  $\pm 50\%$  and measuring the percentage effect propagated to the ultimate calculation of curvature (Fig. 8). Due to the nonlinear nature of the equations involved in the model, the sensitivity study was done graphically, since the calculation of partial derivatives with respect to various parameters would offer only infinitesimal sensitivity about the mean values. This study demonstrated that the model was most sensitive to  $\alpha_1$ , the thermal expansion coefficient, and to  $h_2$ , the height of the transversus/verticalis muscle layer. A +50% change in  $\alpha_1$  resulted in a +51.8% change in curvature,  $k_b$ ; while a -50% change in  $\alpha_1$  resulting in a -50.6% change in  $k_b$ . Conversely, a +50% change in  $h_2$  resulted in a -39.6% change in  $k_b$ ;

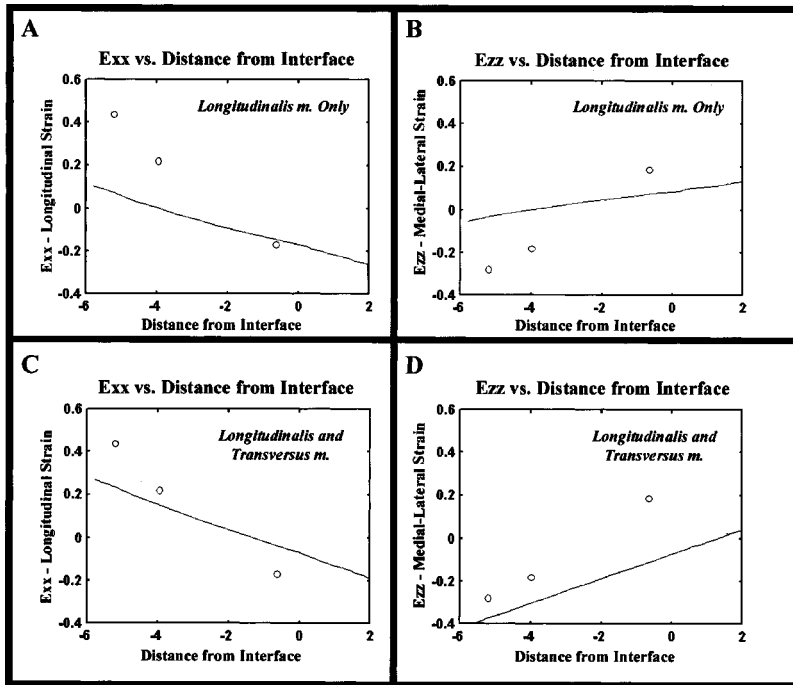


Fig. 7 Modeled strain data (longitudinal strain,  $E_{xx}$ ; and through-plane strain,  $E_{zz}$ ) for both contraction scenarios were computed and graphed versus location along the tongue cross-section. Empirical data points were plotted as circles on the same graph. The synergistic contraction scenario corresponded better to the empirical (Tagging MRI derived) data than did contraction of the longitudinalis muscle alone.

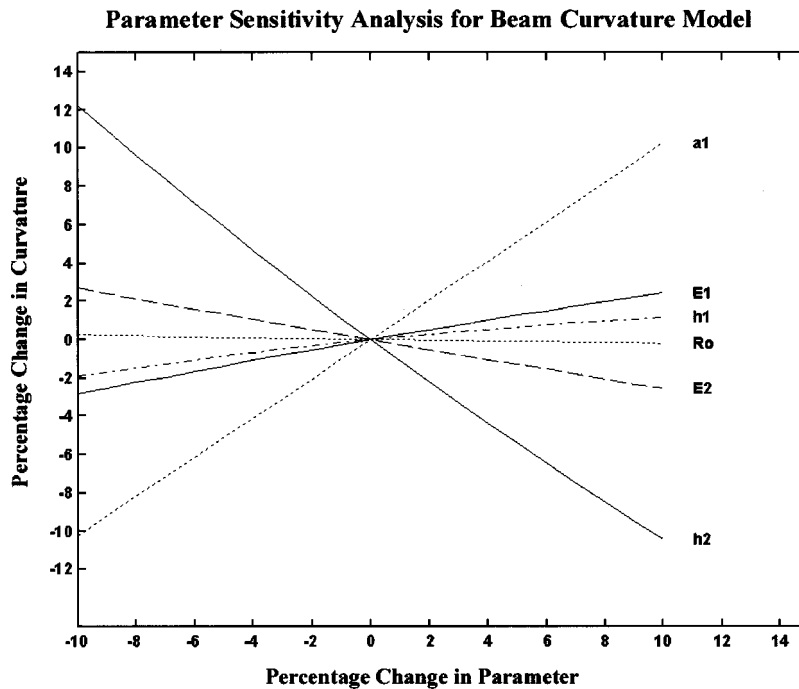


Fig. 8 Sensitivity analysis of the equations involved in the model was completed by finding the effect induced on the computed curvature by varying a given model parameter. Model parameters were varied by  $\pm 10\%$  and percentage effect on curvature was computed throughout. This analysis showed that curvature was most sensitive to  $\alpha_1$  (the thermal expansion coefficient of the beam containing the superior longitudinalis muscle), and  $h_2$  (the height of beam the beam containing the transversus muscle).

while a  $-50\%$  change in  $h_2$  resulting in a  $+85.2\%$  change in  $k_b$ . Hence,  $\alpha_1$  proved to have a direct linear relationship to the curvature (see governing equations), while the variation due to  $h_2$  was inverse and slightly more nonlinear in nature. However, within a more physiological range of  $\pm 10\%$  (a more reasonable range considering parameter measurement errors as well), there was not a single parameter to which the curvature showed hypersensitivity ( $k \propto |cx|^n; n \geq 2$ ), underscoring the stability of the model. The model proved to be less sensitive to the Young's modulus ( $E_1$  or  $E_2$ ), and to  $h_1$ , the height of the longitudinalis muscle layer. The height of layer 1 was less influential than the height of layer 2 because percentage changes of a significantly smaller value ( $h_1 = 2$  mm;  $h_2 = 5.8$  mm) translate to a smaller variability in composite beam height,  $h$  (a summed parameter important for ultimate curvature change). Finally, the model was almost completely insensitive to the initial curvature of the resting tongue (variability of  $k_b$  was less than  $2.5\%$  for a  $50\%$  change in  $R_o$ ). This variable had a greater effect on the calculated final curvature through equation (9).

While the analog model adequately approximated sagittal tongue bending, offering insight into the contractions involved, there were several assumptions adopted during the modeling effort which need discussion. In regard to model development, the assumption that planar sections remain planar, i.e. that there was no shear deformation, reflected our idealization of sagittal bending. In fact, the MRI data [3] showed that postero-inferior muscular attachments of the anterior tongue constrain the bending deformation, leading to the development of finite shear strains. Because this shear strain was external in nature, and did not arise directly from intrinsic muscular contraction, it was neglected in the model. Future iterations of our model will incorporate various boundary conditions (such as the postero-inferior attachment of the genioglossus muscle) and shear accommodating Timoshenko beams, rather than Bernoulli-Euler beams. Another assumption made in the development of the model was that the synergistic effects of longitudinalis and transversus muscle contraction could be combined by the theory of superposition [23]. The theory of superposition states that strains arising from various multi-dimensional stresses can be combined by summation as long as the constitutive relations are in a linearly elastic range. Hence, in order to explore synergistic effects in this modeling effort it was important to model the constitutive properties of the bimetal strip with isotropic linear elastic definitions. Since our model was static (bimodal—either deformed or undeformed) and did not include dynamic behavior (viscoelasticity, calcium homeostasis, dependence of stretch reflex on shortening speed, or reflex delays), we felt that this assumption was adequate. This assumption was also made in several previous lingual modeling efforts [9,10,24,25]. Furthermore, while exact constitutive data does not exist for the various heterogeneous regions of the human tongue, the musculature is most definitely skeletal muscle, for which there did exist limited constitutive property data in the case of isotropy. Another option would have been to assume orthotropy for the beam elements (due to the symmetry planes of the longitudinalis and transversus/verticalis muscles). However, we chose not to do this due to a lack of adequate experimental constitutive data, and due to the fact that our sensitivity study demonstrated that the model was not particularly sensitive to Young's modulus.

Regarding the definition of model parameters, data derived from MRI (such as  $b, L, h, k_o$ ) were deemed sufficiently robust as all were derived from the same subject. On the other hand, the longitudinalis and transversus cross-sectional composition percentage values were taken from the online Visible Human database, and thus were likely to have a higher degree of measurement and applicability error as they came from an unrelated cadaver. Nonetheless, it is a fair assumption that the relative myofiber composition is stable within a species, especially for gender matched individuals. Finally, it should be noted that the contraction scenarios studied involved maximal muscular contractions. In reality, maximal tetanic tension is rarely reached in a physiologic system.

This assumption was considered appropriate for our scenarios due to the fact that the deformation studied was a relatively extreme motion, and maximal muscular effort would have been approached.

One of the most significant insights derived from the current modeling study was the paramount role muscular synergy played in creating tissue deformation. For example, during anterior protrusion (a highly functional, if sometimes culturally offensive, act), the transversus, verticalis, and even the extrinsic genioglossus muscle play active contractile roles [3,10]. In light of our modeling results, we hypothesize that the superior longitudinalis muscle also acts in concert with the above muscle groups to straighten the tongue from its resting bent configuration. Though subtle, this action is nevertheless functionally important, and illustrates the physiological reliance of synergistic muscular synchrony in the regulation of tissue deformation. This phenomenon further supports the concept of the tongue as a muscular hydrostat. Another example of the synergistic interplay of the tongue's muscular elements is the retrograde thrusting of the posterior tongue during the bolus propulsion stage of the swallow. This maneuver is important in clearing the bolus from the oral cavity into the oropharynx. Previous investigations found that bolus propulsion results from synergistic contraction of the posterior transversus muscle, as well as by external traction from the styloglossus muscle [18]. Conceivably, such redundancies are important to assure physiological success, even if one of the contractile elements becomes dysfunctional due to disease or trauma. As in other biomechanical manipulator systems in nature, synergistic muscular contractions augment physiological motion and add support and rigidity to the system. From a teleological perspective, muscular synergy may represent a necessary adaptation for life-sustaining functions, such as feeding, control of the respiratory tract, and communication.

Despite the large impact of lingual disorders on the health and well-being of patients with neurological disease [26,27], there is remarkably little known of the underlying mechanical mechanism for these disorders. Our approach conceptualizes global lingual deformation in terms of the aggregate effect of the multiple local strain events occurring throughout the tissue during physiological movement. This approach should allow us to characterize the intramural mechanical defect associated with impaired lingual force production in patients. This will, in turn, guide therapy specific to the mechanical defect and provide a more rational basis for surgical planning.

## Appendix 1. Non-linear Strain Definition

The derivation of Green's strain definition for bending strain in a curved beam undergoing bending was based on several geometric manipulations. Non-linear bending strain for a curved beam (Fig. A1) was defined on the basis of the fact that the angle,  $\phi_b$ , which relates the rotation of a cross-sectional plane induced by the bending moment, can be expressed by

$$\phi_b = L_o \left( \frac{1}{R_b} \right) \quad (A1.1)$$

where  $L_o$  is the arc length at the neutral axis and  $R_b$  is the radius of curvature caused by the bending moment. The axial deflection,  $\delta$ , of the arc length  $L$  at a distance  $y$  from the neutral axis can then be expressed as

$$\delta = y \phi_b = y L_o \left( \frac{1}{R_b} \right) \quad (A1.2)$$

Thus, the stretch at a distance,  $y$ , from the neutral axis can be expressed:

$$U = \frac{L + \delta}{L} = 1 + y \frac{L_o}{L} \left( \frac{1}{R_b} \right) \quad (A1.3)$$

Finally, noting through geometric similarity that

$$\frac{L_o}{L} = \frac{R_o}{R} = \frac{R_o}{R_o + y} \quad (A1.4)$$

Green's strain definition,  $\varepsilon = 1/2(U^2 - 1)$ , can be applied to define non-linear bending strain in a curved beam using the following definition:

$$\varepsilon = \frac{1}{2} \left[ \left( 1 + \frac{yR_o}{y+R_o} \left( \frac{1}{R_b} \right) \right)^2 - 1 \right] \quad (A1.5)$$

## Appendix 2. Finding the Neutral-Axis in a Curved Beam

It is important to note that for an initially curved beam undergoing elastic bending, the neutral axis does not pass through the centroid of cross-sectional area, but is displaced toward the center of initial curvature [12]. Mathematically, the neutral axis is found by setting the total (integrated) axial force over the cross-section equal to zero:

$$P = \int \sigma dA = 0 \quad (A2.1)$$

Assuming a linearly elastic material, and the absence of a large deviation from the neutral axis for large deformations, equation (A2.1) can be expanded as:

$$\int E(R - R_o) \frac{R_o}{R} \left( \frac{1}{R_b} \right) dA = 0 \quad (A2.2)$$

where  $R$  is the radius of curvature to any material point on the cross section,  $R_o$  is the radius of curvature at the neutral axis,  $R_b$  is the radius of curvature produced by the moment. This equation can then be simplified, assuming that  $R_b$  and  $R_o$  do not vary over the cross-section:

$$\int \frac{R - R_o}{R} dA = 0 \quad (A2.3)$$

or

$$\int dA - R_o \int \frac{dA}{R} = 0 \quad (A2.4)$$

which can be rearranged to yield an expression for the radius of curvature of the neutral axis:

$$R_o = \frac{A}{\int \frac{dA}{R}} \quad (A2.5)$$

Hence, for the cross-sectional geometry assumed by the tongue model, the neutral-axis can be solved for explicitly:

$$R_o = \frac{h}{\ln \left( \frac{R_2}{R_1} \right)} \quad (A2.6)$$

where  $R_2$  is the convex side radius, and  $R_1$  is the concave side radius.

## References

- [1] Miyawaki, K., 1974, "A Study of the Musculature of the Human Tongue," Annual Bulletin of the Research Institute of Logopedics and Phoniatrics, University of Tokyo, **8**, pp. 23–50.
- [2] Smith, K. K., and Kier, W. M., 1989, "Trunks, Tongues, and Tentacles: Moving with Skeletons of Muscle," *Ann. Sci.*, **77**, pp. 29–35.
- [3] Napadow, V. J., Chen, C., Wedeen, V. J., and Gilbert, R. J., 1999, "Intramural Mechanics of the Human Tongue in Association with Physiological Deformations," *J. Biomech.*, **32**, pp. 1–12.
- [4] Matthys, L., and DeMey, G., 1996, "An Analysis of an Engineering Model for the Thermal Mismatch Stresses at the Interface of a Uniformly Heated Two Layer Structure," *Int. J. Microcircuits Electron. Packag.*, **19**, pp. 323–329.
- [5] Suhir, E., 1989, "Interfacial Stresses in Bimetal Thermostats," *J. Appl. Mech.*, **56**, pp. 595–600.
- [6] Timoshenko, S., 1925, "Analysis of Bimetal Thermostats," *J. Opt. Soc. Am.*, **11**, pp. 233–255.
- [7] Chiel, H. J., Carago, P., Mansour, J., Hathi, K., 1992, "Biomechanics of a Muscular Hydrostat: A Model of Lapping by a Reptilian Tongue," *Biol. Cybern.*, **67**, pp. 403–415.
- [8] Wilhelms-Tricarico, R., 1995, "Physiological Modeling of Speech Production: Methods for Modeling Soft Tissue Articulators," *J. Acoust. Soc. Am.*, **97**, pp. 3085–3098.
- [9] Hashimoto, K., and Suga, S., 1986, "Estimation of the Muscular Tensions of the Human Tongue by using a Three-dimensional Model of the Tongue," *J. Acoust. Soc. Jpn. (E)*, **7**, pp. 39–46.
- [10] Sanguineti, V., Laboissiere, R., and Payan, V., 1997, "A Control Model of Human Tongue Movements in Speech," *Biol. Cybern.*, **77**, pp. 11–22.
- [11] Mu, L., and Sanders, I., 1999, "Neuromuscular Organization of the Canine Tongue," *Anat. Rec.*, **256**, pp. 412–424.
- [12] Shanley, F., 1957, *Strength of Materials*, McGraw-Hill Book Company, Inc., New York.
- [13] Visible Human Project Web Site-<http://www.nlm.nih.gov/research/visible>.
- [14] Duck, F. A., 1990, *Physical Properties of Tissue: A Comprehensive Reference Book*. Academic Press, London.
- [15] Matsumoto, Y., 1967, "Validity of the Force-Velocity Relation for the Muscle Contraction in the Length Region,  $1 < l_0$ ," *J. Gen. Physiol.*, **50**, pp. 1125–1137.
- [16] Elliott, G. F., Lowy, J., Worthington, C. R., 1963, "An X-Ray and Light-diffraction Study of the Filament Lattice of Striated Muscle in the Living State and in Rigor," *J. Mol. Biol.*, **6**, pp. 295–305.
- [17] Abbott, B., and Baskin, R., 1962, "Volume Changes in Frog Muscle during Contraction," *J. Physiol. (London)*, **161**, pp. 379–391.
- [18] Napadow, V. J., Chen, Q., Wedeen, V. J., Gilbert, R. J., 1999, "Biomechanical Basis for Lingual Muscular Deformation During Swallowing," *Am. J. Physiol.*, **277**, pp. G695–701.
- [19] Niitsu, M., Kumada, M., Campeau, N. G., Niimi, S., Riederer, S. J., and Itai, Y., 1994, "Tongue Displacement: Visualization with Rapid Tagged Magnetization-Prepared MR Imaging," *Radiology*, **191**, pp. 578–580.
- [20] Axel, L., and Dougherty, L., 1989, "MR Imaging of Motion with Spatial Modulation of Magnetization," *Radiology*, **171**, pp. 841–845.
- [21] Young, A. A., and Axel, L., 1992, "Three-dimensional Motion and Deformation of the Heart wall: Estimation and Spatial Modulation of Magnetization—A Model-based Approach," *Radiology*, **185**, pp. 241–247.
- [22] Zerhouni, E. A., Parish, D. M., Rogers, W. J., Yang, A., and Shapiro, E. P., 1988, "Human Heart: Tagging with MR Imaging—A Method for Noninvasive Assessment of Myocardial Motion," *Radiology*, **169**, pp. 59–63.
- [23] Crandall, S., 1959, *An Introduction to the Mechanics of Solids*, McGraw-Hill Publications, New York.
- [24] Kakita, Y., and Fujimura, O., 1977, "Computational Model of the Tongue: A Revised Version," *J. Acoust. Soc. Am.*, **62**, pp. S15(A).
- [25] Kiritani, S., Miyawaki, K., Fujimura, O., and Miller, J. E., 1976, "A Computational Model of the Tongue," Annual Bulletin, Research Institute of Logopedics and Phoniatrics, University of Tokyo, **10**, pp. 243–251.
- [26] Weijnen, F. G., Kuks, J. B., van der Bilt, A., van der Glas, H. W., Wassenberg, M. W., and Bosman, F., 2000, "Tongue Force in Patients with Myasthenia Gravis," *Acta Neurol. Scand.*, **102**, pp. 303–308.
- [27] Robbins, J., Logemann, J., and Kirshner, H., 1986, "Swallowing and Speech Production in Parkinson's Disease," *Ann. Neurol.*, **19**, pp. 283–287.